Of Multilayer Films by X-Ray Diffraction

M.R. Behfrooz[*]

Department of Physics, Islamic Azad University of Mahabad, Mahabad, Islamic Republic of Iran

Abstract

X-ray diffraction measurements were performed on $Co_\alpha Pt_{1-\alpha}$/Pd, Co/Pd, Co/Fe, and Co/W multilayer samples with different structures, such as $Co_\alpha Pt_{1-\alpha}$ alloy layer composition α, bilayer thickness, and number of bilayers. Multilayer samples were made by magnetron sputtering in a chamber with multi-parallel guns and a position controllable substrate. $Co_\alpha Pt_{1-\alpha}$ alloy layers were deposited by cosputtering from Co and Pt targets mounted on guns tilted towards a common substrate. Compositions of Co and Pt in $Co_\alpha Pt_{1-\alpha}$ layers were varied by use of different sputtering power. The thicknesses of magnetic and non-magnetic layers in multilayered samples were also systematically changed to investigate the relationship between X-ray diffraction lines and crystalline structures of multilayered films. It was found that the position of the main diffraction peak from multilayered films was solely determined by the crystalline structures within bilayers rather than bilayer thickness. A model was introduced to calculate microstructural parameters such as the thickness of interfaces and compositions at interfaces.

Keywords: Multilayer films; X-Ray diffraction; $Co_\alpha Pt_{1-\alpha}$/Pd; Co/Pd; Co/Fe; Co/W

Introduction

Multilayered films fabricated in different deposition systems, such as molecular beam epitaxy, electron beam evaporation, and magnetron sputtering, have attracted much attention in the last decade because of their novel magnetic, optical, and mechanical properties [1,2]. Particularly due to the application to high density magneto-optic recording media, magnetic multilayers of Co/Pt and Co/Pd [3-7] have been intensively studied. In the last few years, more than 20 non-magnetic materials making up multilayers with either Co or Fe have been investigated world wide. Of these materials, (Co or Fe)/(Pt, Pd, Au, Ag, Cu, Cr, Dy, Gd, or Tb) are the most popular. In order to get perpendicular magnetic anisotropy which is crucial for magneto-optic recording media, the thickness of magnetic layers (Co or Fe) is limited to about 3Å. Therefore, powerful microstructural analysis tools such as high resolution electron microscopy (HRTEM) are necessary to study nanostructures of multilayers. However, in most cases, because the interesting regions in multilayered systems are interfaces which are no more than 10Å thick, one may not be able to obtain details of the nano-structure of these multilayers, even with HRTEM.

X-ray diffraction (XRD) is another powerful and convenient tool that has been used in scientific science for many years. Recently, because of new materials

*E-mail: mr.behfrooz@mail.urmia.ac.ir

fabrication techniques, artificial structures have been the focus of many research groups. These developments challenge the XRD technique, and new interpretations of XRD data are required. Lots of works have been done on XRD from multilayered systems by many groups such as Fullerton and Schuller *et al* [8]. But because in XRD only the scattered X-ray intensity is measured and the phase information is totally missing, modeling is usually required to fit the measured intensity, and thus indirectly, the structures of samples may be obtained. The problem with modeling is that fits are not unique.

In general, low angle XRD from multilayered structures has been fairly well understood, and at least qualitative descriptions of structures can be determined. Fullerton *et al.* [8] have successfully built models that fit low angle X-ray diffraction patterns, as well as large angle XRD patterns, to get information on layer interface sharpness. However, the interpretation of wide angle peaks remains unclear in some cases, especially for ultra-thin sublayer multilayers, and there still exist many open questions. In particular, positions of wide angle peaks appear to be in question when they are used to interpret crystalline structures, because the position of peaks may be changed by the artificial layering. Therefore crystalline structures and material phases in multilayered films may not always be directly found from wide angle XRD patterns alone.

For one-dimensional ideal superlattices where all the atomic layers are parallel and there are no interdiffusions and no layer thickness fluctuations the following model describes the diffracted X-ray intensity from the superlattices [13,14]:

$$I = I_0 \left(\frac{\sin(NqL/2)}{\sin(qL/2)} \right)^2 \left[\left(f_1 \frac{\sin(n_1 q d_1/2)}{\sin(q d_1/2)} \right)^2 \right.$$

$$+ \left(f_2 \frac{\sin(n_2 q d_2/2)}{\sin(q d_2/2)} \right)^2$$

$$+ 2 f_1 f_2 \cos\left(\frac{q}{2}(L + d_1 - d_2) \right)$$

$$\left. \left(\frac{\sin(n_1 q d_1/2) \sin(n_2 q d_2/2)}{\sin(q d_1/2) \sin(q d_2/2)} \right) \right) \right]$$

where N is the number of bilayers; q is the wave vector; $d_1(d_2)$ is the lattice spacing of the first (second) sublayers; $n_1(n_2)$ is the number of atomic planes in the first (second) sublayer; $f_1(f_2)$ is the atomic scattering factor of the first (second) sublayer. For multilayers consisting of ultra-thin sublayers (3-20Å) with many bilayers, the first term in the above equation dominates, and the positions of all diffraction peaks are basically

determined from this term. However, for multilayers made in sputtering and thermal evaporation systems, interdiffusions at interfaces are unavoidable and alloys may form at interfacial regions. Furthermore, layer thickness fluctuation is another factor that can eliminate the superlattice effects for XRD peaks at large angle [9,10]. This study was conducted in order to study systematically this problem and, thus, to obtain a clear understanding of how the structures (including layer thickness, number of layers, and interdiffusivity between layers) influence the diffraction results.

There are many samples made for this study. In sections §1 and §2, we report on multilayers with different layer structures and different interfacial crystallinities, and study crystalline structures of these films. In section §3, a simple model is employed to determine microstructural parameters, such as interface thickness and composition at interfaces, based on measured quantities such as bilayer thickness and film composition. These microstructural parameters, in general, are not easy to be directly measured. We found that the model is useful in the sense that important parameters such as local composition and relative atomic number density may be estimated. As mentioned above, XRD alone may not always yield unique and complete solutions to all the microstructural parameters. Other independent measurements must be made to uniquely determine these parameters. We found that for Co/Pd multilayers, magnetic measurements were helpful for the determination of microstructural parameters. Magnetic measurement data are presented in section §4. More detailed study on magnetic properties of some of these samples has been carried out and will be published elsewhere.

Experimental

Multilayers were grown in a multi-gun magnetron sputtering system with each gun oriented in an upward direction and a substrate positionable above the desired gun. Base pressure of the system was 5×10^{-8} Torr. Sputtering pressure was 5 mTorr of Ar gas. The $Co_\alpha Pt_{1-\alpha}$ alloy layers were fabricated by cosputtering from Pt and Co targets which were tilted at an angle so that Pt and Co would be deposited simultaneously on the substrate.

According to their structures, the $Co_\alpha Pt_{1-\alpha}/Pd$ samples were divided into four groups: In Group I, the nominal structure of the samples was $Co_\alpha Pt_{1-\alpha}(17\text{Å})/Pd(3.3\text{Å}) \times 20$, and the composition α of Co varied from about 8.5 to 36 atomic percent estimated from energy dispersive spectroscopy (EDS). In Group II, the structure was $Co_{0.2}Pt_{0.8}(\beta\text{Å})/Pd(3.3\text{Å}) \times 20$, and layer thickness β varied from 9 to 29Å. In Group III, the

number of bilayers τ was changed from 10 to 40, and the bilayer structure was kept the same: $Co_{0.2}Pt_{0.8}$ (21Å)/Pd(3.3Å). In Group IV, the thickness of Pd sublayers γ was changed from 3.3 to 19.8Å with other parameters fixed: $Co_{0.2}Pt_{0.8}(21Å)/Pd(\gamma Å)x20$.

The structural parameters of these samples are summarized in Table 1. Alloy films $Co_\alpha Pt_{1-\alpha}$ with α ranging from 20 atomic percent Co to 28 atomic percent Co were also made for comparison purpose. Conventional θ-2θ X-ray diffraction was performed and both small and large angle scans were taken.

For samples of Co/Pd (Group V), Fe/Pd(Group VI), and Co/W(Group VII) multilayers, the thicknesses of the Co or Fe layers varied from a fraction of one mono-layer(1Å nominally) to about 4Å. The nonmagnetic layers such as Pd and W had fixed layer thickness of 13Å, as shown in Table 2. There were seven samples in each group. Because of the different diffusivity between Co-Pd, Fe-Pd, and Co-W, these three groups were made for the study of the interdiffusion and its effect on XRD patterns.

There were two other sample groups (VIII and IX). These were used to test a model that relates micro-structural parameters, such as interfacial thickness, to measurable quantities such as bilayer thickness and over-all composition. The sample structural parameters are listed in Tables 3 (Group VIII) and 4 (Group IX). The bilayer thickness λ *of* these samples and the over-all composition of Co x were determined from small angle XRD and EDS, respectively.

Results and Discussion

§1. $Co_\alpha Pt_{1-\alpha}$/Pd Multilayers

In this section, XRD results from multilayers made with $Co_\alpha Pt_{1-\alpha}$ alloy layers and Pd layers will be discussed. The structures of these samples can be found in Table 1.

In sample group I of $Co_\alpha Pt_{1-\alpha}$/Pd multilayers, the composition of the Co in $Co_\alpha Pt_{1-\alpha}$ sublayers varies from 8.5 atomic percent to 36 atomic percent. Small angle XRD patterns from these samples reveal that the bilayer thickness of the samples is about 24Å compared with the nominal thickness of about 20Å. Up to the third order for small angle peaks are visible for these samples. From this information, it can be concluded qualitatively that these samples have similar layered structures or chemical modulation. In the large angle region, there are a few peaks visible: peaks labeled (111), (200), (311), and (222) as shown in Figure 1 for $Co_\alpha Pt_{1-\alpha}$/Pd with α=0.085 (sample I-1). The (220) peak is also clearly visible for samples with Co concentration

Table 1. The general structure is $[Co_\alpha Pt_{1-\alpha}(\beta Å)Pd(\gamma Å)]x\tau$. The parameters in parentheses indicate the variable parameters of the groups. Parameters assigned values indicate fixed parameters in the group

Sample number	Group I(α) β=17 γ=3.3 τ=20	Group II(β) α=0.2 γ=3.3 τ=20	Group III(τ) α=0.2 β=21 γ=3.3	Group IV(γ) α=0.2 β=21 τ=20
1	0.085	9	10	3.3
2	0.159	13	15	6.6
3	0.195	17	25	9.9
4	0.255	21	30	13.2
5	0.283	25	35	16.5
6	0.359	29	40	19.8

Table 2. Co/Pd (Group V), Fe/Pd (Group VI), and Co/W (Group VII) multilayer sample groups. In each group, the non-magnetic sublayer (Pd or W) is 13Å thick nominally, and the thickness of the magnetic sublayer (Co or Fe) varies from a fraction of one mono-layer (1Å) to about two atomic layers (4Å)

Sample number	1	2	3	4	5	6	7
λ_{Fe} or λ_{Co}(Å)	1	1.5	2	2.5	3	3.5	4

Table 3. Sample (Group VIII) structures of Co(2Å)/Pd(λ_{Pd})x35 multilayers. The bilayer thickness λ and over-all composition of Co x were measured using small angle XRD and energy dispersive spectroscopy

Sample number	1	2	3	4	5	6	7
λ_{Pd} (Å)	4	7	10	13	16	19	21
λ (Å)	6.6	10.1	13.1	15.5	18.9	21.2	24.9
$Co_x Pd_{1-x}$	0.37	0.24	0.18	0.15	0.13	0.11	0.10

Table 4. Sample (Group IX) structures of Co(4Å)/Pd(λ_{Pd}) with total film thickness of about 300Å. Bilayer thickness λ and Co composition x were measured using small angle XRD and EDS

Sample number	1	2	3	4	5	6
λ_{Pd}	4	8	12	16	20	24
No. of bilayers	37	25	18	15	12	10
λ(Å)	10.8	15.5	20.8	25.2	30.0	34.5
$Co_x Pd_{(1-x)}$	0.56	0.45	0.37	0.32	0.25	0.23

a less than 25 atomic percent. The position of these peaks varies corresponding to the change of Co concentration α, as shown in Figure 2. These large angle peaks clearly reveal polycrystalline fcc structures with differing lattice parameters. In this case, the bilayer thickness has a negligible effect on the large angle peak positions. This may indicate that there does not exist strong coherence between layers, or as other groups have pointed out, [9,10] superlattice peaks do not exist when there are layer thickness fluctuations.

XRD patterns from samples of group II (see Table 1) show the same result (not shown) that the change of bilayer thickness has virtually no effect on the position of large angle peaks for these sputter deposited multilayer films. These results suggest that for Group II, chemical modulation of the films has no effect on the position of the large angle peaks. The intensity of these peaks increases with increase in layer thickness, as expected. The above results and discussions suggest that layered structures fabricated in sputtering system have little effect on positions of large angle peaks. Crystalline structures of films are the dominant factors determining large angle diffraction patterns.

XRD data from Groups III and IV show the same results from a different angle. Samples in group III have different number of bilayers, varying from 10 to 40. Group IV samples have different Pd layer thicknesses. The total film thickness, therefore, increases for samples in both Groups III and IV. The intensity of peaks increases accordingly. In general, the reflected X-ray intensity from *(hkl)* planes is proportional to the effective volume of the sample,[11] and in this case, proportional to the film thickness. In both sample groups III and IV, the intensity of (111) and (222) peaks increases faster than others, indicating that the preferred direction to grow is with (111) planes parallel to the film surface. Figure 3 shows the positions of the (222) peaks from samples in Group IV. It can be seen that although the Pd layer thickness increases from about 3Å to 20Å, the (222) peak does not move at all. It once again shows that chemical modulation length has little effect on the position of large angle peaks. Other results are that satellite peaks appear clearly when the nominal Pd sublayer is more than 10Å thick, as shown in Figure 4. For ideal multilayer structures, satellite peaks always exist, however, in practice, because of the layer thickness fluctuation of each individual layer, satellite peaks are visible only when thickness fluctuations are small compared with each individual layer thickness. Thus, the existence of satellite peaks may indicate small layer thickness fluctuations.

§2. Co/Pd, Fe/Pd, and Co/W

In this section, XRD from Co/Pd, Fe/Pd, and Co/W multilayers will be discussed. When two different materials are mixed together, there is always a certain type of solid state reaction between the two materials if they are miscible. It is expected that when multilayers are grown, alloy layers between layers could be formed. Therefore, interdiffusion between layers is a very interesting phenomenon. Samples listed in Table 2 have differing known interdiffusivity for these materials. These samples have about the same chemical modulation, as expected and shown by small angle
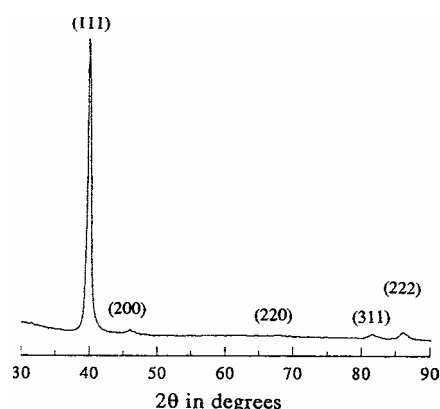

Figure 1. A typical large angle diffraction pattern from sample I-1. The peaks show that the film has fcc structure.
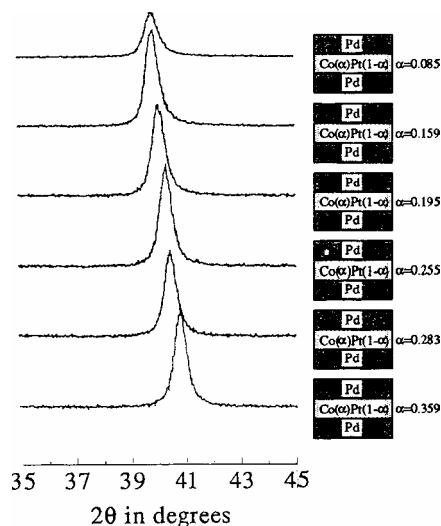

Figure 2. Diffraction patterns from samples in group I of Table 1. The shift of the peak corresponds to the lattice structural changes due to alloying.

XRD scans in Figure 5, since they all have the same nominal structure. However, diffraction peaks from these samples at large angle behave differently. Figure 6 shows (111) peaks from Co/Pd samples with structures listed in Table 2. Notice that the peak shifts when the thickness of the Co layer increases, and that the peak intensity increases as well.
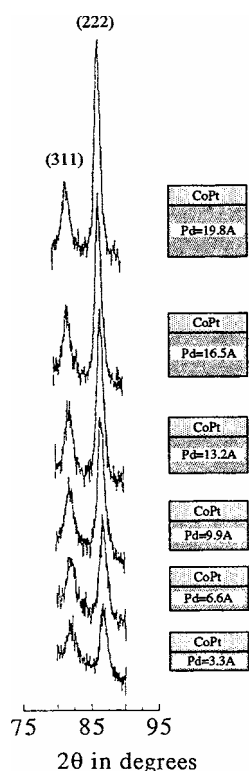
On the other hand for Fe/Pd multilayers also listed in Table 2, the diffraction peak shifts just as for the Co/Pd samples, but the peak intensity goes down when the Fe layers are getting thicker and thicker, as shown in Figure 7. The change of the diffraction intensity is directly related to microstructure of thin films. The phase diagram of Co and Pd shows no intermetallic compound formation in the entire composition range. Instead, Co and Pd will form a solid solution at any composition of Co in Pd. However, Fe and Pd do have a chance to form an intermetallic compound such as FePd or $FePd_3$. Therefore, the formation of compounds which may not be chemically ordered at interfaces may reduce the grain size, which will cause the diffraction peak broadening. The small shift of the peak position may be explained in two ways. One is that the d-spacing
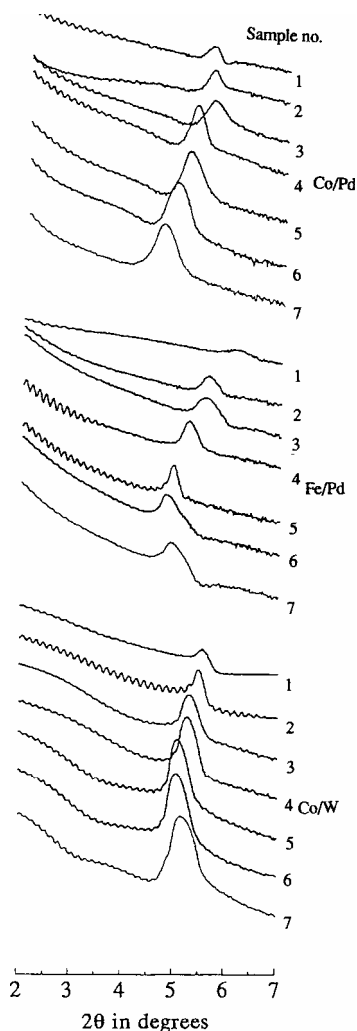

Figure 3. Diffraction patterns from (311) and (222) planes of samples in Group IV of Table 1. The peaks do not move when Pd layer thickness changes.
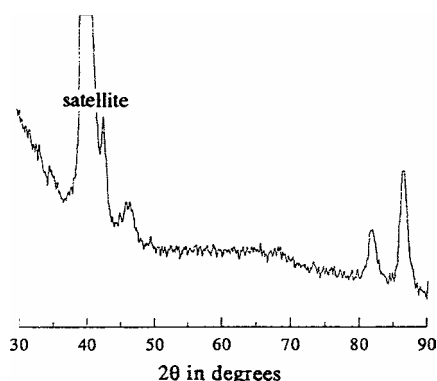
Figure 4. Satellite peaks show up on the right side of the main peak when the Pd layer thickness is more than 10Å. (Sample IV-3, Table 1).

Figure 5. Small angle XRD patterns from Co/Pd(top), Fe/Pd (middle), and Co/W(bottom). (See Table 2).

detected is the average d-spacing of the two sublayers. When one layer is getting thicker, the average weight of the d-spacing of that layer will be greater. Thus, the detected d-spacing will move towards the value of that d-spacing. This explanation is valid for multilayers with rather thick sublayers. In that case, the layers are thick enough to grow with their bulk structures. Another explanation is that for multilayers containing ultrathin sublayers, such as the samples in this study, the two sublayers of a bilayer are only about several Å, or three to four mono-layers thick. For such a small amount of material, it is difficult to form structures the same as for bulk. For samples of either Co/Pd or Fe/Pd multilayers, because the similarity in crystallinity of Pd layers (fcc) and CoPd or FePd alloy layers (also fcc), it is impossible to draw any conclusion about crystalline structures in different layers. In fact, it is likely that the lattice structure of the two sublayers are the same, and entire film takes on the crystal structure of the thicker sublayer.

The lattice structure of W (bcc) is entirely different from that of CoW alloys which were made by co-sputtering, as shown in Figure 8. The XRD from sputter deposited W films shows the typical bcc structure. By adding about 10 at % Co in W, a different XRD pattern
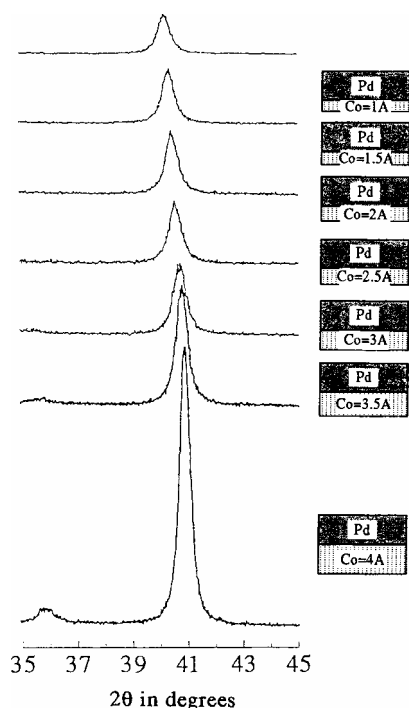
shows up. Also, when the composition of Co increases, the intensity of the main peak reduces, and finally, the peaks disappear, as shown in Figure 8. The Co/W multilayers behave exactly the same as these CoW alloy films, as shown in Figure 9. The only difference is that the peak at about 2θ=40° is more intense for the multilayers. Also when the Co layers get thick enough (>4Å), the entire film becomes amorphous.

Now, there are some difficulties explaining the Co/W XRD patterns using the idea of an average d-spacing, because the diffraction pattern from W does not have a peak around 2θ=35°. As a matter of fact, it is quiet clear
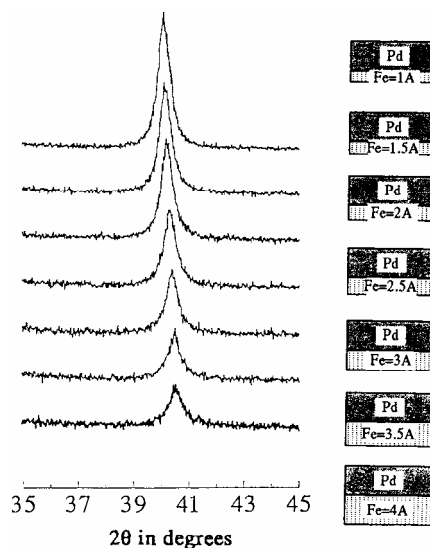

Figure 7. Large angle XRD patterns from Fe/Pd multilayers. Notice that the peak shifts and gets less intensive when Fe layer thickness increases. (See Table 2).
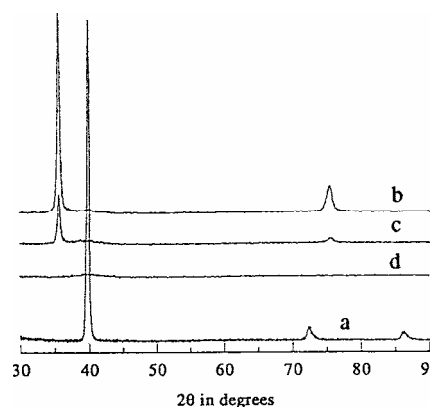

Figure 8. XRD patters of W (a) and CoW alloys (b: 10 at. % Co, c: 14 at. % Co and d: 17 at. % Co). These patterns show that additional of small amount of Co entirely changes film crystalline structures.

Figure 6. Large angle XRD patterns from Co/Pd multilayers. Notice that the peak shifts and gets more intensive when Co layer thickness increases. (See Table 2).

that the entire film of Co/W multilayers should possess the same lattice structure. So far, the type of lattice structure in either CoW alloy films or in Co/W multilayers has not been identified because there is not enough information. In order to get more diffraction peaks from these Co/W samples, and thus, to identify the phase, grazing incident angle X-ray diffraction may be useful [12]. From Co/W samples, it can be seen that interdiffusion between the Co and W sublayers is so significant that a trace (1Å) of Co will change the entire lattice structure. On the other hand, these Co/W multilayers are still chemically modulated, as shown in Figure 5.

From the above analysis and discussions of the microstructures of ultra-thin sublayer multilayers made by sputter deposition, it can be concluded that the entire film possesses the same lattice structure, but atoms of the two materials are distributed in such a way that chemical modulation still exists in the direction perpendicular to surface, as shown schematically in Figure 10.
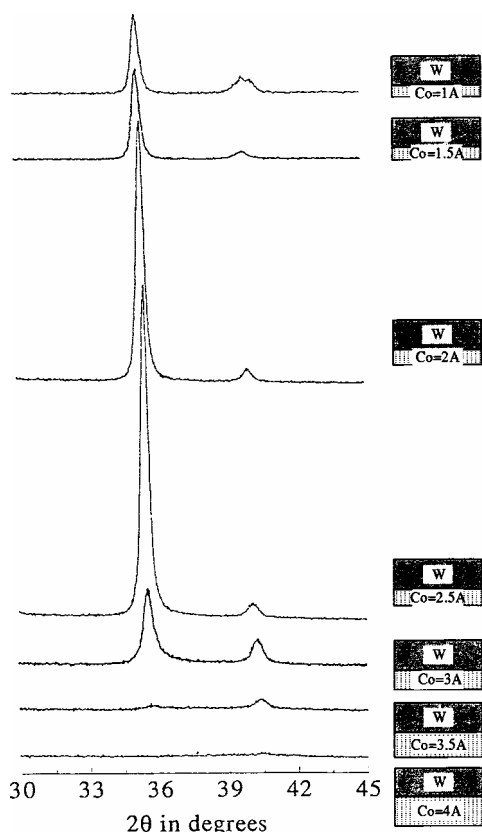
As mentioned previously, a quantitative micro-structural description of multilayers with ultra-thin sublayers, such as samples in this study, is very difficult to obtain. Fittings to X-ray diffraction patterns usually ends up with more than one possible solution which may be equally physical. Therefore, more information from measurements other than XRD is required to uniquely determine microstructures. In order to make use of the information from other measurements, a relation between quantities obtained from XRD and that from other measurements is desired. To this end, we propose the following simple model which will lead to an equation relating quantities, such bilayer thickness and over-all composition of the entire film to microstructural parameters such as interracial thickness and local composition.

§3. Modeling of Interfaces

The model is shown schematically in Figure 11. The figure shows one of bilayers in a X/Y multilayer system containing materials X and Y. Sublayers a and b are determined in such a way that layer a contains both X and Y, and layer b contains only Y. In other words, layer a is the layer of X and Y mixture, and layer b is pure Y. After defining a few other parameters (such as local composition of X in layer a: $x(X)_a$; and atomic numbers per volume in layers a and b: n_a and n_b), the following equation is obtained:
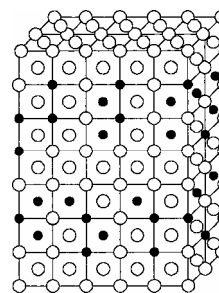

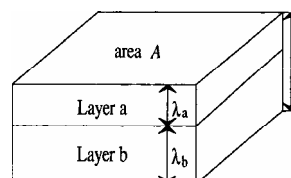**Figure 10.** A schematic of crystalline structure consisting of ultra-thin sublayers.

Figure 11. A model relating microstructural parameters, such as interface thickness, to measurable quantities, such as bilayer thickness and over all composition.

Figure 9. Large angle XRD patterns from Co/W multilayers. Notice that the similarity of these patterns and those of CoW alloy films shown in Figure 8. (See Table 2).

$$\lambda = \lambda_a \left(1 - \frac{n_a}{n_b}\right) + \frac{n_a}{n_b} \lambda_a x \left(X\right)_a \frac{1}{x\left(X\right)}$$

where λ is the bilayer thickness, λ_a a sublayer thickness, $x(X)$ over-all composition of X.

In order to test the correctness of the model and the equation, two groups (VIII and IX) of Co/Pd samples were made, and nominal and measured parameters concerning these sample structures are listed in Tables 3 and 4. One common point for these samples is that the nominal Co layer thickness is constant, and that deposition conditions such as sputtering pressure and sputtering power are the same for all samples. Therefore, it is expected that all samples within each group have the same interfacial structure. This means that if λ *vs.* $1/x$ (Co) is plotted, a straight line is expected. For samples listed in Tables 3 or 4, a line is indeed obtained, as shown in Figures 12 and 13. For the line in Figure 12 where λ *vs.* $1/x$ (Co) of samples in Table 3 is plotted, the intercept and slope can be easily calculated and their values are -0.134Å and 2.45Å for the intercept and slope, respectively. Because there are three unknown parameters: λ_a, $x(Co)_a$, and n_a/n_b, and only two equations, these three unknowns still cannot be uniquely determined. Therefore, other measurements to independently determine one of the three unknowns is required, as presented below.

The validity of the above equation can be verified by assuming a special case where the local composition $x(Co)_a$ is 1. That means that there is no interdiffusion between Co and Pd sublayers. Then, the nominal values of Co and Pd sublayer thickness should be recovered. It is found that in the case of $x(Co)_a=1$, λ_a is 2.11Å, very close to the nominal value of 2Å. The nominal value of 4Å Co layers for Co/Pd samples in Table 4 is also recovered when the special case of $x(Co)_a=1$ is assumed.

§4. Magnetic Measurements

Magnetic measurements were made on samples listed in Table 3. It turns out that the magnetic measurements are helpful to independently determine the interfacial layer thickness. The saturation magnetization σ_S of these samples are plotted *vs.* the nominal Pd layer thickness in Figure 14. Because of the induced moments on Pd atoms near Co atoms, the σ_S initially increases. It means that some of the 12 nearest neighbors of Pd atoms are Co atoms. When the Pd layer thickness increases, σ_S increases, indicating that the added Pd atoms still have some Co atoms as neighbors. σ_S keeps increasing until the Pd layer thickness reaches a value of about 10Å, as

shown in Figure 14. Therefore, the Pd atoms added after the layer thickness reaches about 10Å make no contribution to the magnetization. This indicates that Co atoms do not diffuse farther than 5Å in either direction.

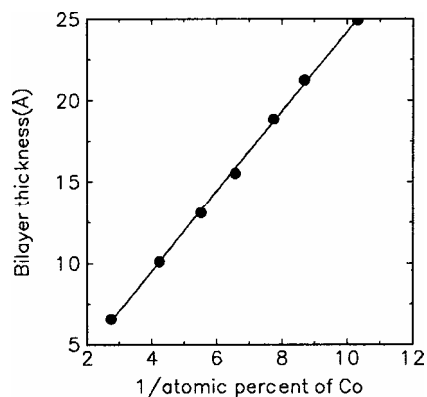**Figure 12.** Bilayer thickness λ *vs.* inverse of over-all Co composition of samples listed in Table 3.
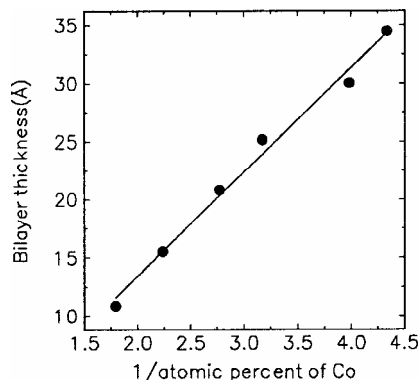

Figure 13. Bilayer thickness λ *vs.* inverse of over-all Co composition of samples listed in Table 4.
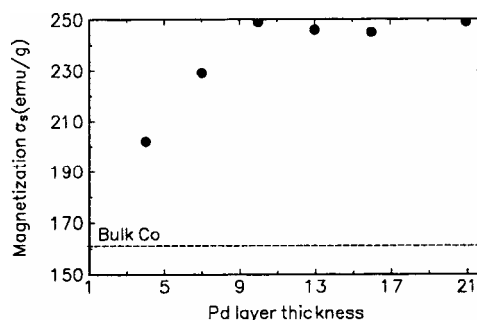

Figure 14. Saturation magnetization σ_S *vs.* nominal Pd sublayer thickness. Data from samples in Group VIII listed in Table 3. σ_S is calculated using Co mass only.

From this experiment, it can be estimated that the Co-Pd mixing layer is about 12Å thick. Based on this estimation, the other two parameters in the above equation can be calculated: x(Co)a=20 at. % Co, and n_a/n_b=1.026.

Some comments should be made about the above analysis. First, the local composition x(Co)a is the average value for sublayer *a*. Second, the atomic number ratio n_a/n_b is very close to 1 but greater than 1, indicating that the average size of atoms in the a layers is slightly smaller than those in the *b* layers which is the case for Co/Pd multilayers. Finally, we point out that there is no crystalline structure information involved in the model, therefore the model should be equally applicable to amorphous multilayers. This model is applicable to multilayers with one very thin sublayer.

Summary

Multilayers consisting of ultra-thin sublayer were studied. It has been found that for sputter deposited multilayers, the chemical modulation along the perpendicular direction to the surface does not affect the diffraction line positions at large angle. Because of interdiffusion and alloying effects at interfaces, the lattice structure of the entire film tends to take the same form. The chemical modulation remains as the result of the deposition procedure. A simple model has been introduced to relate microstructural parameters such as interfacial layer thickness and local composition to measurable quantities such bilayer thickness and overall composition.

References

1. Gibson J.M., Osbourn G.C., and Tromp R.M. *Materials Research Society Symposia.* 56 (2001).
2. Falicov L.M., Pierce D.T., *et al. J. Mater. Res.*, **5**: 1299 (1998).
3. Sato N. *J. Appl. Phys.*, **64**: 6424 (1988).
4. Ochiai Y., Hashimoto S., and Aso K. *lEEE-Tran. Mag.*, **25**: 3755 (2001).
5. Carcia P.F., Shah S.I., and Zeper W.B. *Appl. Phys. Lett.*, **56**: 2345 (1990).
6. He P., McGahan W.A., Woollam J.A., Sequeda F., McDaniel T., and Do H. *J. Appl.Phys.*, **69**: 4021 (1991).
7. He P., McGahan W.A., Nafis S., Woollam J.A., Liou S.H., Shan S.Z., Sequeda F., McDaniel T., and Do H. *Ibid.*, **70**: 6044 (1991).
8. Fullerton E.E., Schuller I.K., Vanderstraeten H., and Bruynseraede Y. *Phys. Rev. B.*, **112**: 3056 (1999).
9. Clemens B.M. and Gay J.G. *Ibid.*, **35**: 9337 (1998).
10. Hollanders M.A. and Thijsse B.J. *J. Appl. Phys.*, **70**: 1270 (1991).
11. Cullity B.D. *Elements of X-Ray Diffraction.* Addison-Wesley Publishing Co. (1978).
12. Bowen D.K. and Matyi R. XRD Workshop of 41st Denver X-Ray Conference. Colorado Springs, Co., August 3-7, (1998).
13. Garaces Y. and Sanchez H. Thin Solid Films. **355**: 487 (1999).
14. Ohring M. *The Materials Science of Thin Films.* Academic, SanDiego, CA, 126 (2001).